Femtosecond-laser sharp shaping of millimeter-scale geometries with vertical sidewalls

Qiuchi Zhu, Peixun Fan, Nan Li, Timothy Carlson, Bai Cui, Jean-François Silvain, Jerry L. Hudgins, Yong Feng Lu

International Journal of Extreme Manufacturing

Femtosecond-laser sharp shaping of millimeter-scale geometries with vertical sidewalls

OPEN ACCESS
IOP Publishing | IMMT
International Journal of Extreme Manufacturing
Int. J. Extrem. Manuf. 3 (2021) 045001 (12pp)
https://doi.org/10.1088/2631-7990/ac2961

Femtosecond-laser sharp shaping of millimeter-scale geometries with vertical sidewalls

Qiuchi Zhu[1,4], Peixun Fan[1,4,*], Nan Li[1], Timothy Carlson[1], Bai Cui[2], Jean-François Silvain[3], Jerry L Hudgins[1] and Yong Feng Lu[1,*]

[1] Department of Electrical and Computer Engineering, University of Nebraska, Lincoln, NE 68588, United States of America
[2] Department of Mechanical and Materials Engineering, University of Nebraska, Lincoln, NE 68588, United States of America
[3] CNRS, University of Bordeaux; Bordeaux I.N.P., ICMCB, UMR 5026, F-33608 Pessac, France

E-mail: ylu2@unl.edu and fanpeixun@gmail.com

Received 9 July 2021, revised 29 August 2021
Accepted for publication 23 September 2021
Published 18 November 2021

Abstract

As femtosecond (fs) laser machining advances from micro/nanoscale to macroscale, approaches capable of machining macroscale geometries that sustain micro/nanoscale precisions are in great demand. In this research, an fs laser sharp shaping approach was developed to address two key challenges in macroscale machining (i.e. defects on edges and tapered sidewalls). The evolution of edge sharpness (edge transition width) and sidewall tapers were systematically investigated through which the dilemma of simultaneously achieving sharp edges and vertical sidewalls were addressed. Through decreasing the angle of incidence (AOI) from 0° to −5°, the edge transition width could be reduced to below 10 μm but at the cost of increased sidewall tapers. Furthermore, by analyzing lateral and vertical ablation behaviors, a parameter-compensation strategy was developed by gradually decreasing the scanning diameters along depth and using optimal laser powers to produce non-tapered sidewalls. The fs laser ablation behaviors were precisely controlled and coordinated to optimize the parameter compensations in general manufacturing applications. The AOI control together with the parameter compensation provides a versatile solution to simultaneously achieve vertical sidewalls as well as sharp edges of entrances and exits for geometries of different shapes and dimensions. Both mm-scale diameters and depths were realized with dimensional precisions below 10 μm and surface roughness below 1 μm. This research establishes a novel strategy to finely control the fs laser machining process, enabling the fs laser applications in macroscale machining with micro/nanoscale precisions.

Supplementary material for this article is available online

Keywords: femtosecond laser, extreme manufacturing, millimeter-scale machining, zero-taper drilling, edge quality control

1. Introduction

Higher precisions are a major goal being continuously pursued in most modern manufacturing techniques. Nowadays, micro/nanoscale precisions have been achieved through different methods but primarily for microscale geometries [1–3]. Machining macroscale geometries above millimeters

[4] Contributed equally to this work.
[*] Authors to whom any correspondence should be addressed.

2631-7990/21/045001+12$33.00

(mm) while keeping precisions at micro/nanoscales is still a remaining challenge.

Femtosecond (fs) laser machining has attracted increasing interest in various fields due to its unique advantages of being noncontact, material-independent, flexible, and having low thermal effects. As fs lasers of high pulse energies and repetition rates are emerging, their machining capabilities are being continuously pushed to new boundaries including smaller features, larger scales, higher resolutions, and higher efficiencies [4–7]. Significant advances have been realized in machining extremely small geometries (e.g. below 50 nm [8, 9]). Nevertheless, achieving micro/nanoscale precisions in both shapes and dimensions with fs lasers when machining macroscale geometries is more challenging in critical industrial fields, such as the manufacturing of injection nozzles in engines [10, 11] and cooling holes on turbine blades [12, 13].

In fs laser machining, achieving micro/nanoscale precisions becomes more difficult at larger overall sizes due to more complex machining routes and more significant influences from the defocusing of laser beams [14, 15]. For example, both tapered sidewalls and poor-quality edges form when machining macroscale holes (e.g. diameters and depths $\geqslant$1 mm) using fs lasers through conventional two-dimensional (2D) galvo scanners or translation stages (figures 1(a)–(j)), which are the two major obstacles to reaching high precisions (e.g. <10 μm) [16–22]. Significant research efforts have been made to investigate separate parameters (e.g. laser power, scan speed, focal positions, angle of incidence (AOI), hatching paths, ambient environment, etc), with optimal processing conditions being identified [18–22].

Over the past decade, the ability to flexibly control the scanning of laser beam has significantly improved, in particular, due to the development of five-axis (5-axis) scanners (figure 1(b)), permitting tuning of sidewall tapers from positive (i.e. entrances > exits) to negative (i.e. entrances < exits) [10, 23, 24]. Our preliminary experiments showed that sidewalls with near-zero tapers can be produced even at an AOI of 0° when proper fs laser conditions were used through a 5-axis scanner. However, poor-quality edges with rough chamfers at the entrances are yet to be addressed (figures 1(e), (h) and (k)), particularly when machining deep holes ($\geqslant$1 mm) where the movement of fs laser focal spots along the depth direction (i.e. the *Z*-direction) is inevitable. Strategies to simultaneously realize both vertical sidewalls and sharp edges are highly demanded for achieving micro/nanoscale precisions in macroscale machining.

In this research, we developed an fs laser sharp shaping approach (figure 1(c)) to machining macroscale holes of various geometries using a 5-axis scanner. The underlying mechanisms for the formation of poor-quality edges and sidewall tapers were revealed. For the first time, the fs laser ablation behaviors in actual manufacturing were flexibly controlled, through which a parameter-compensation strategy was developed to improve the sidewall and edge qualities in fs laser machining. Through tuning the AOI and implementing the parameter compensation (by gradually decreasing the scanning diameters and using optimal laser powers), we simultaneously achieved vertical sidewalls as well as sharp hole entrances and exits (figures 1(f), (i) and (l)). Apart from round holes, geometries of different shapes with both mm-scale lateral dimensions and depths were also achieved, with dimensional precisions below 10 μm and surface roughness below 1 μm. In addition to AOI which is most commonly used to tune tapers, this research indicates that controlling the fs laser ablation behaviors via parameter compensation can also realize tuning of sidewall tapers from positive to negative. This strategy demonstrates the capability of fs lasers in macroscale machining in addition to its prominent advantages in micro/nanoscale manufacturing.

2. Experiments

The fs laser machining was conducted using an Amplitude Tangor laser, which operates at a central wavelength of 1030 nm and a pulse duration of $\sim$ 408 fs. As a widely used engineering material, SAE 304 stainless steel was selected as a typical example in this research. The specimens were square plates measuring 1 $\times$ 1 in^2 with a thickness of 0.91 mm. The linearly polarized laser beam firstly passed through a beam conditioning unit (SCANLAB GmbH) and was transformed to circular polarization. Subsequently, the circularly polarized laser beam was scanned and focused to a spot of $\sim$20 μm in diameter via a precSYS 5-axis micromachining system (SCANLAB GmbH), which can modify the AOI in a range of $-7.5°$ to $+7.5°$. During the laser machining, compressed air was continuously fed through a nozzle attached to the precSYS 5-axis system as an assisting gas to eject residues from laser ablation.

We developed a two-step approach to machining geometries with macroscale dimensions (e.g. holes with both a 1 mm diameter and a 1 mm depth) with clean edges, as shown in figure 2. In Step 1, the fs laser was rotated along spiral circles with a speed of 50 Hz (rounds per second) in the *X*–*Y* plane. At each depth position, the entire-hole-area was repeatedly filled with spiral circles for 25 times (Process 1). Then, the fs laser focal spot was forwarded 100 μm along the *Z*-direction to the next depth position (Process 2). After reaching the targeted depth, the laser focal spot was moved back to the entrance to conduct another machining cycle (i.e. Processes 1 and 2). In total, four machining cycles were conducted in Step 1 and, thus, the entire-hole-area was filled with spiral circles for 100 times (25 $\times$ 4) at each depth position. Herein, the target depth was set to be $\sim$400–500 μm in Step 1, which was sufficient for machining through 1 mm-deep holes. In Step 2, helical scanning was performed continuously throughout the entire sidewalls (with a revolving distance of 1 μm and a rotating speed of 200 Hz) and repeated for 250 times. Step 1 was designed to achieve complete material removal to facilitate Step 2. Step 2 was performed as a high-speed refining process to realize smoother sidewalls and sharper, cleaner edges with fewer depositions and debris.

In Step 2, the helical scanning diameters were set to be 20 μm smaller than the designed diameters. The scanning diameters in Step 1 were either consistent at different

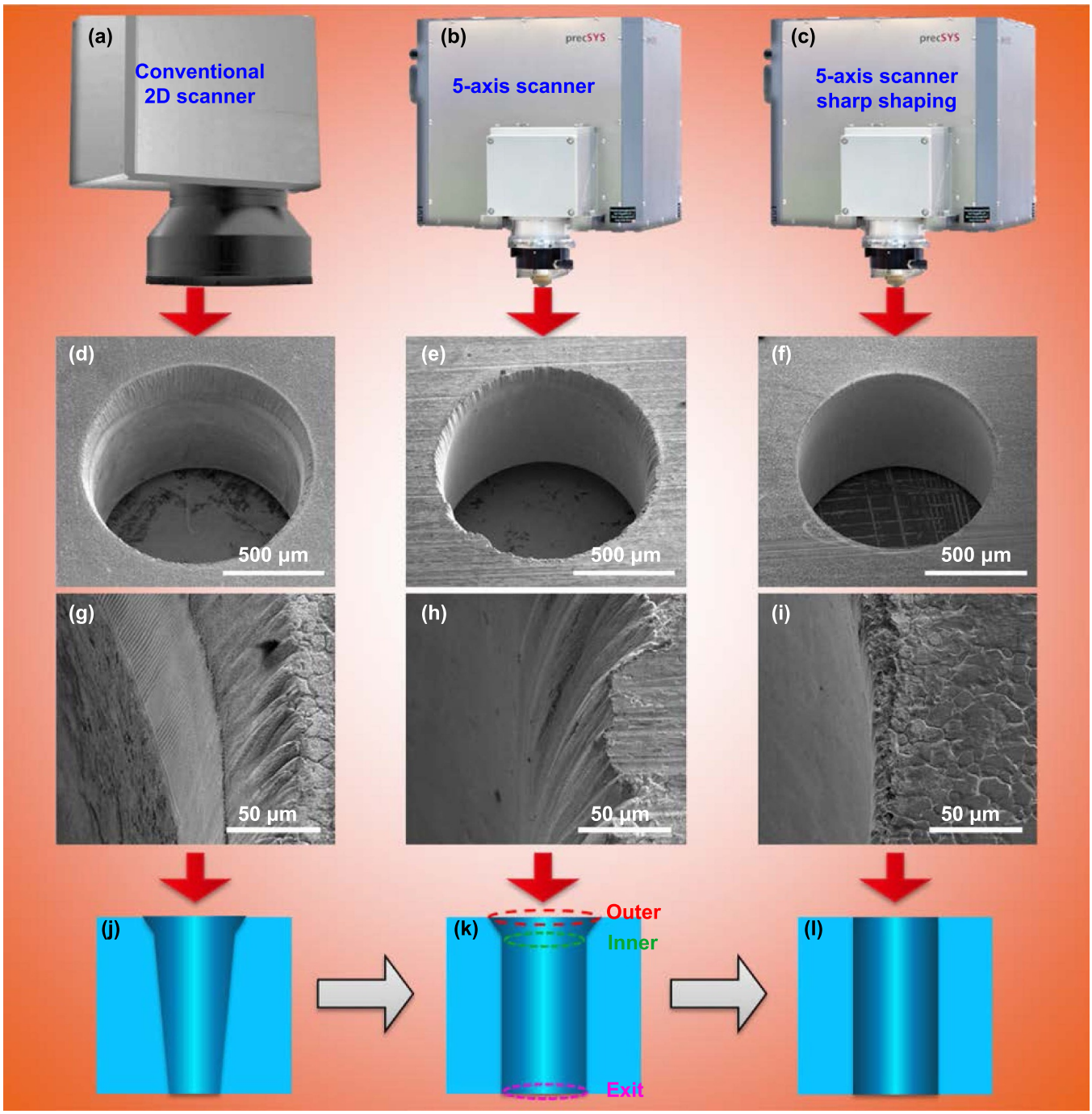

Figure 1. (a)–(c) Different machining approaches and (d)–(i) the corresponding typical machining results. (d)–(f) 30°-tilted scanning electron microscopy (SEM) images for holes machined by different approaches. (g)–(i) Magnified SEM images at the edges of (d)–(f), respectively. (j)–(l) Schematics of cross-sections of holes machined by the different approaches.

depth positions or gradually reduced from the entrances to deeper positions. Regardless of the specific diameter values, the maximum spiral circles in Step 1 were set to be 45 μm smaller than the scanning diameters in Step 2 at the same depth position throughout the entire depth. The preliminary experiments identified that a pulse repetition rate of 110 kHz and a laser power below 9.8 W can render the machining of high-quality holes of 1 mm diameter and 1 mm depth. Therefore, the pulse repetition rate was kept constant at 110 kHz, while the laser average power was adjusted in a range of 2.5–9.8 W to achieve higher machining precisions. The SEM images were collected by an FEI Helios NanoLab 660 Dual Beam scanning electron microscope. The dimensions of the geometries machined at both their entrances and exits were measured from their SEM images using the ImageJ software. The three-dimensional (3D) images of the machined geometries were collected using a Keyence VK-X200K laser scanning microscope.

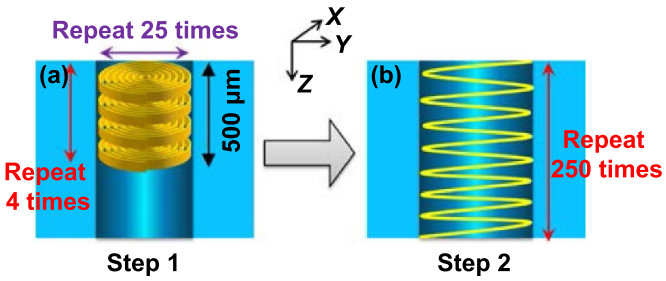

Figure 2. Schematics of the two-step machining approach: (a) step 1, the complete material removing process via laser rotating along spiral circles; (b) step 2, the high-speed refining process via continuous helical scanning.

3. Results and discussion

3.1. Mechanism underlying the formation of poor-quality edges

The mechanism underlying the formation of poor-quality edges was first investigated. For holes shallower than the laser focal depth, the entire hole can be machined without forwarding the laser focal spot along the Z-direction, leaving the machined hole free from the influence of laser defocusing. However, machining deeper holes beyond the machining capability of the fs laser within a single focal plane requires the Z-direction movement of the laser focal spot, resulting in the re-machining of the entrances under defocusing conditions and consequently the poor-quality edges.

To verify this, we gradually forwarded the fs laser focal spot from the top surfaces of the samples ($Z = 0$ μm) to a depth position of 400 μm with the AOI fixed at 0°. As presented in figures 3(a1)–(a3), the entrances were initially sharp when laser machining was conducted at the surfaces. As the laser focal spot moved deeper, rough edges appeared at the entrances with increased chamfers, as shown in figures 3(b1)–(c3), indicating the occurrence of the laser machining at defocusing conditions. More detailed results for $Z = 0$, 100, 200, and 400 μm are shown in figure S1 (available online at stacks.iop.org/IJEM/3/045001/mmedia).

Since beam divergence is the main consequence of laser defocusing, the poor-quality edges are expected to be reduced after correcting beam divergence. As a comparison, the maximum AOI provided by the 5-axis micromachining system (i.e. AOI $= -7.5°$) was used when the laser focal spot was forwarded to a depth of 400 μm. As shown in figures 3(d1)–(d3), clean and sharp entrances are achieved without noticeable chamfers, confirming the dominant role the beam divergence plays in causing the defects on edges in macroscale machining.

To examine the decrease in defects on edges with AOI, round holes of the same diameter were machined using the same laser parameters and forwarding depth ($Z = 400$ μm) but with AOIs being varied by a step of 1°. The low-magnification images in figure 4 indicate that an obvious ring-like feature appears on the entrances at an AOI of $-1°$, decreases at an AOI of $-3°$, and becomes unnoticeable at an AOI of $-5°$. The zoomed-in images in figure 4 clearly show that the edges become sharper and smoother as larger AOIs are used. More detailed results for AOI $= -1°$, $-2°$, $-3°$, $-4°$, and $-5°$ can be found in figure S2.

3.2. Influence of AOI on both edge quality and sidewall taper

To quantify the influence of the AOI, the entrance and exit diameters of the holes machined at different AOIs were measured at various orientations and averaged, as shown in figure 5(a). The edge transition widths (edge widths for short, i.e. the differences between the outer and inner radii of the entrances) and the sidewall tapers were analyzed, as plotted in figure 5(b). The edge width was used in this research to evaluate the defects on the edges of entrances. With larger AOIs, the outer diameters of the hole entrances obviously decreased while the inner diameters of entrances showed only slight changes (figure 5(a)). Consequently, the edge widths evidently decreased from above 50 μm at an AOI of 0° to below 10 μm at an AOI larger than $-5°$ (figure 5(b)). Meanwhile, the exit diameters obviously increased (figure 5(a)), resulting in larger sidewall tapers (figure 5(b)).

The cross-sectional schematics in figure 5(a) illustrate the evolution of the hole shapes as larger AOIs are used. Vertical sidewalls (i.e. the inner diameters of the entrances almost equal the exit diameters) can be achieved at small AOIs (e.g. AOI $= 0°$). However, obvious edges were produced at the entrances. Controlling the AOI can reduce edges but results in increased sidewall tapers. It is difficult to simultaneously control the outer and inner entrance diameters and the exit diameters to the same value within an error range of 10 μm. Therefore, producing vertical sidewalls with sharp edges cannot be realized by simply controlling the AOI.

To solve the dilemma of difficulties in achieving sharp edges and vertical sidewalls simultaneously, the fs laser ablation behaviors were further analyzed. As illustrated in figure 6(a), the overall ablation can be considered to be composed of the vertical and lateral ablation (i.e. along the depth and radial directions for round holes) at oblique incidences. The vertical ablation is for machining deeper holes while the lateral ablation is for increasing hole diameters. When a constant scanning diameter is used at oblique incidences, the laser ablation occurs vertically and laterally at the same time, causing cone-shaped holes with negative sidewall tapers. Although the vertical ablation is always the major part of the overall ablation at small AOIs, the lateral ablation increases at larger AOIs, resulting in larger sidewall tapers. Since the AOI is necessary to achieve sharp edges, preventing lateral ablation at oblique incidences is the key to vertical sidewalls. Accordingly, two specific parameters were carefully adjusted to compensate for lateral ablation (i.e. the scanning diameter and the laser power), with a parameter-compensation strategy developed for sharp shaping geometries with vertical sidewalls. The edge widths are nearly identical at AOIs of $-5°$, $-6°$, and $-7°$ but the sidewall tapers increase continuously (figure 5(b)). Therefore, an AOI of $-5°$ was selected as the optimal value in this research for suppressing defects

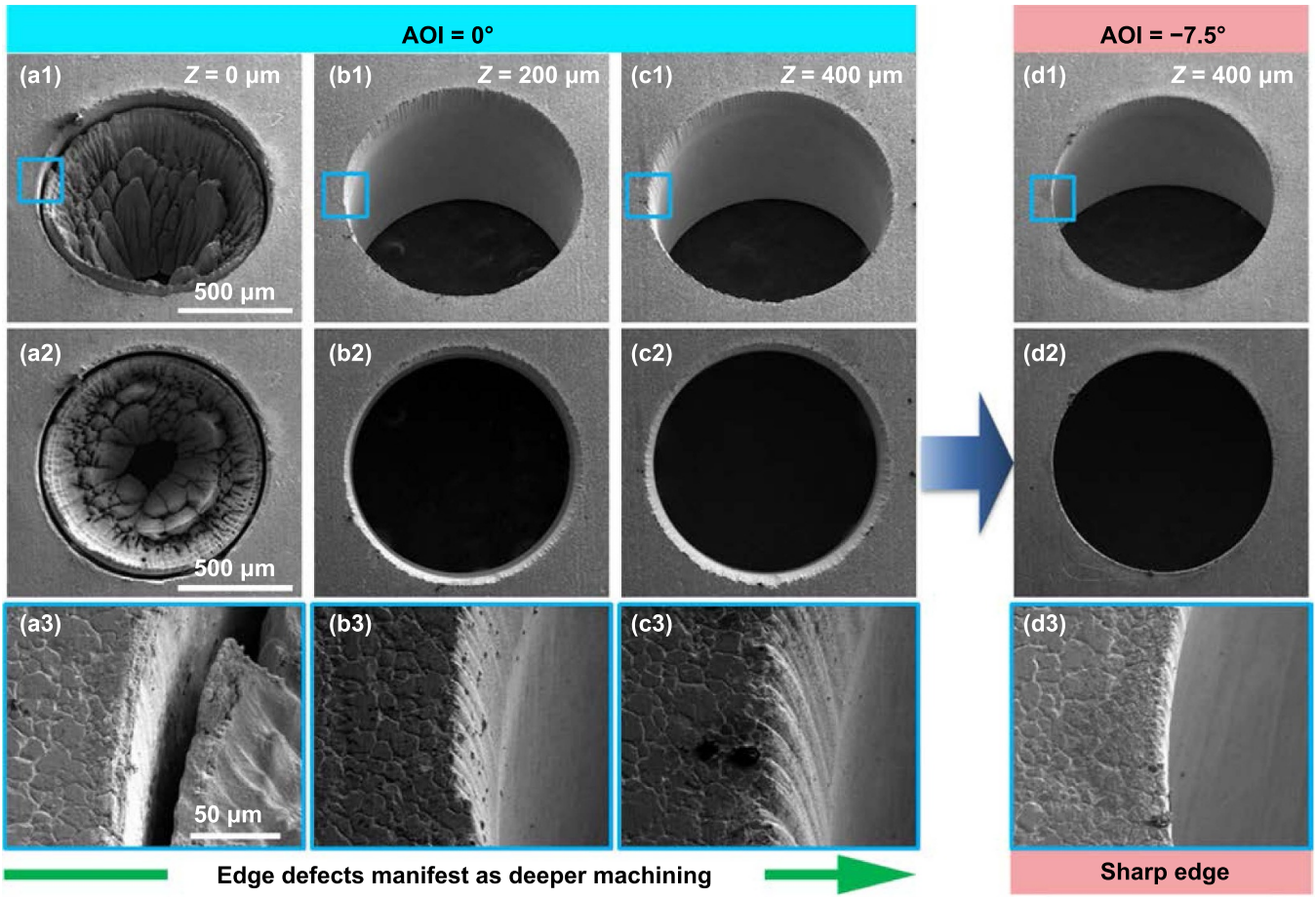

Figure 3. Influence of machining depth on edge quality. (a1)–(c1) 30°-tilted SEM images of holes produced at an AOI of 0° when the fs laser focal spot was kept at the surface ($Z = 0$ μm), forwarded to 200 and 400 μm depths, respectively. (a2)–(c2) are the top-view SEM images, and (a3)–(c3) are the magnified SEM images of (a1)–(c1), respectively. As a comparison, (d1)–(d3) present the SEM images of the hole produced at a −7.5° AOI when the fs laser focal spot was forwarded to $Z = 400$ μm.

on edges, and it is used in the following discussions. According to the manual of the precSYS system, the typical divergence angle of focused beam is ∼0.08 rad (i.e. ∼4.6°), which is close to the optimal AOI value extracted from the experiments above. It indicates that the defects on the edges of entrances were largely determined by the beam divergence and also influenced by actual manufacturing processes (e.g. shapes and dimensions of geometries, machining approaches, laser parameters, etc).

3.3. Parameter-compensation strategy

Gradually decreasing the scanning diameters along the depth (i.e. the laser scanning routes are programmed as inverted cones, as shown in figure 6(b)), is defined as the scanning-diameter compensation (diameter compensation) in this research. The difference between the maximum and minimum programmed scanning diameters is the amount of diameter compensation. In addition, using the optimal laser power is defined as the laser-power compensation (power compensation), as shown in figure 6(c). Both scanning-diameter and laser-power compensations were applied to reduce lateral ablation and ensure that the majority of laser ablation occurs vertically. The scanning-diameter compensation reduces lateral ablation through conducing off-focus ablation at the sidewalls, while the laser-power compensation is based on the dependence of ablation on laser fluences.

As shown in figure 6(d), the scanning-diameter compensation effectively reduces the exit diameters, making them closer to the entrance diameters. However, the effect of scanning-diameter compensation weakens when using larger diameter compensations. When a 100 μm scanning-diameter compensation was used, the difference between the exit and entrance diameters narrowed more than 20 μm. However, when the scanning-diameter compensation was further increased from 100 to 400 μm, the difference between the exit and entrance diameters narrowed less than 20 μm. The limitation of the scanning-diameter compensation can be more clearly seen from the evolution of the sidewall tapers shown in figure 6(e). The sidewall taper decreased from ∼3.6° without diameter compensation to ∼2.7° with a 100 μm diameter compensation but failed to further decrease to below 2.0° even with a 400 μm diameter compensation. It is suggested that the effect of off-focus ablation in reducing lateral ablation is limited, and, hence, scanning-diameter compensation cannot completely eliminate sidewall tapers.

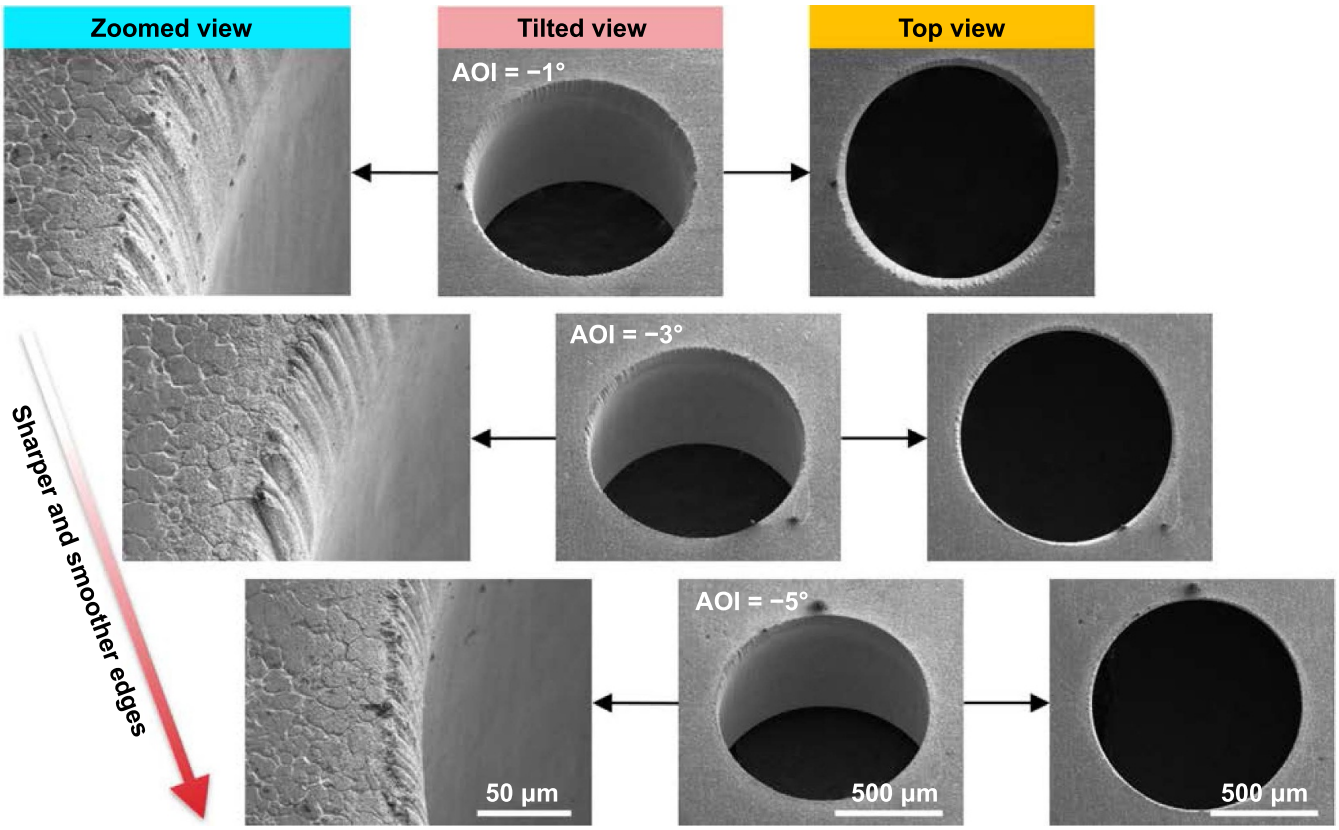

Figure 4. Sharper and smoother edges achieved by decreasing the AOI from -1° to -5°. All holes were produced with the laser focal spot forwarded to a depth of $Z = 400$ μm.

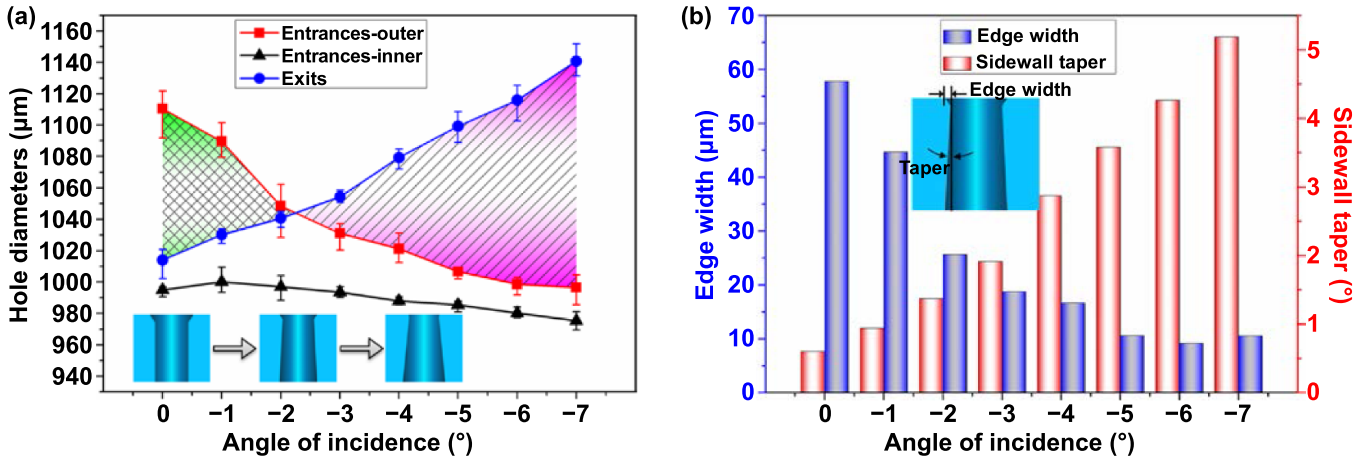

Figure 5. (a) Diameters measured at hole entrances (outer and inner) and exits when different AOIs were used. The insets in (a) indicate the evolution of both entrances and exits with AOIs. (b) Influences of the AOI on the hole edge width and sidewall taper. The inset in (b) is the schematic of the edge width and sidewall taper discussed in this research.

Considering that the laser power has more influence on fs laser ablation, laser-power compensation using optimal laser powers was further implemented. So far, a laser power of 9.8 W was used. When lower laser powers of 7.1 and 5.6 W were used, the exit diameter decreased almost linearly and eventually approached the entrance diameters within an error of 10 μm with a fixed scanning-diameter compensation of 400 μm (figure 6(d)). Accordingly, the sidewall tapers were reduced from 2.3° to 1.3° and then 0.3° at laser powers of 9.8, 7.1, and 5.6 W, respectively (figure 6(e)). The success in achieving nearly non-tapered sidewalls through parameter compensation proves the validity of the analysis on the fs laser lateral and vertical ablation behaviors described above.

In all scanning-diameter and laser-power compensation tests, the outer and inner diameters of the entrances remained at steady levels with a constantly small difference between them (figure 6(d)). As a result, the edge widths were

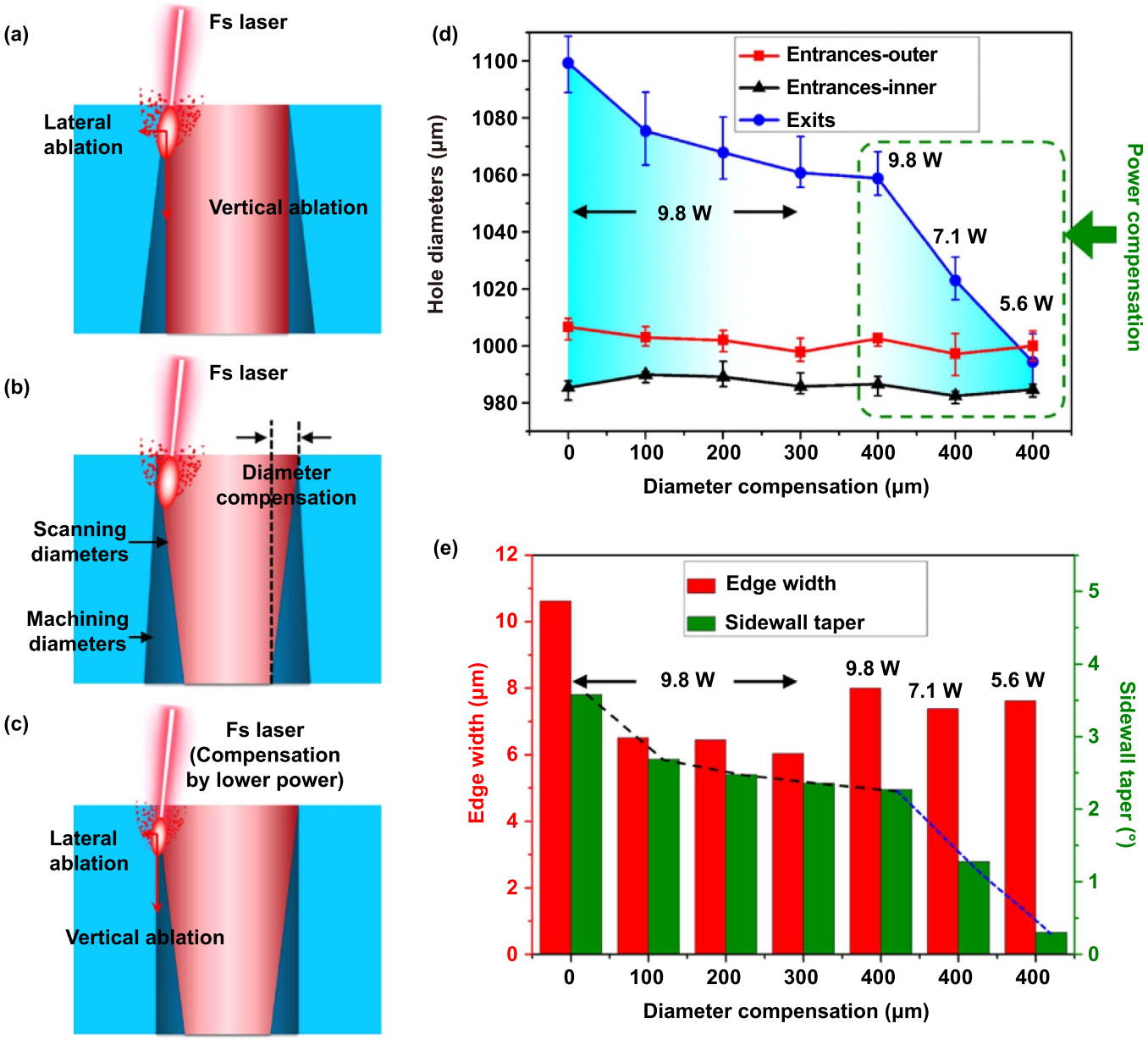

Figure 6. (a)–(c) Schematics of the parameter-compensation strategy: (a) laser machining with unoptimized power and a constant scanning diameter, (b) laser machining with unoptimized power and scanning-diameter compensation, (c) laser machining with both scanning-diameter and laser-power compensations. The red and dark-blue shadows represent the programmed scanning diameters and the machined hole diameters, respectively. The laser focal spot shown in (c) is smaller than that shown in (a) and (b), indicating that a lower laser power was used. (d) Effect of scanning-diameter and laser-power compensation on reducing the diameter differences between the entrances and exits. For machining with diameter compensations of 0–300 μm, a laser power of 9.8 W was used. (e) Influence of parameter compensation on edge width and sidewall taper.

kept below 10 μm independent of the applied parameter compensations (figure 6(e)). Therefore, the AOI control combined with the parameter compensation provides a versatile solution to simultaneously control the edge and sidewall qualities, with sharp edges and vertical sidewalls achieved simultaneously. Here, a 400 μm diameter compensation and a 5.6 W laser power were applied to machine holes with 1 mm diameters and 1 mm depths. The parameter-compensation strategy can be flexibly adjusted for machining macroscale holes of other diameters and depths.

3.4. Flexibility of the parameter-compensation strategy

More details on the influence of laser-power compensation on dimensional precisions are presented in figure 7. Laser powers of 9.8, 8.2, 7.1, 5.6, 4.7, 3.4, and 2.5 W (at a repetition rate of 110 kHz) were separately used to machine the holes of 1 mm diameter and 1 mm depth, with a fixed scanning-diameter compensation of 400 μm. As the laser power decreased from 9.8 to 2.5 W, the exit diameters decreased obviously and monotonically, while the outer and inner diameters of the

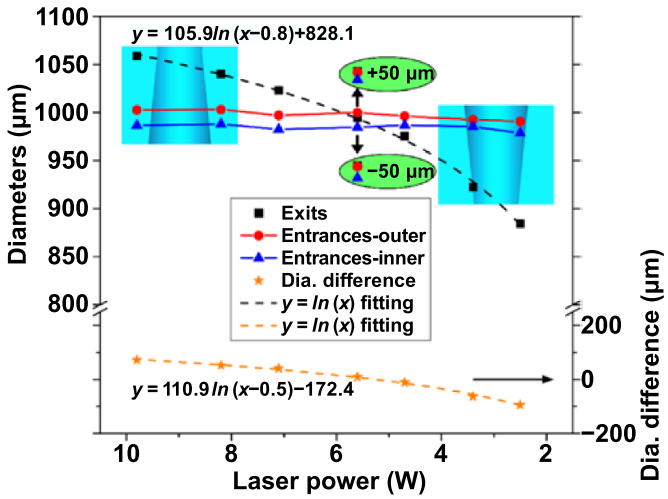

Figure 7. Influences of laser power on the entrance and exit diameters and their differences. The intersection of the black, red, and blue lines indicates the optimal machining condition. Dashed lines are the fitted results showing logarithmic relationships. Circles marked in green are the results measured for two separate holes with diameters 50 μm larger/smaller.

entrances showed no apparent changes. As a result, the exit diameters changed from above to below the entrance diameters as the laser power decreased from higher to lower than 5.6 W, and the profiles of the holes changed from cones to inverted cones. The laser power of 5.6 W produced the least-tapered sidewall for machining 1 mm diameter and 1 mm deep holes at an AOI of $-5°$.

The change of laser power shows little influence on the entrance diameters. At the entrance, the effect of the overall ablation being divided to vertical and lateral portions is insignificant. Therefore, the entrance diameters are mainly determined by the programmed laser scanning routes and slightly influenced by the laser power. The edge widths also stay at a steady level once the AOI is fixed. As the laser machining goes deeper, the effect of lateral ablation accumulates, resulting in negatively tapered sidewalls. When lower laser powers are used as parameter compensations, the lateral ablation decreases more than the vertical ablation since the former is only a small portion of the overall laser ablation (figure 6(c)). Accordingly, the proportion of lateral versus vertical ablation is reduced, producing vertical sidewalls and even inverted-cone holes.

A logarithmic dependence of fs laser ablation on laser fluences (determined by laser power in this research) has been widely identified [25–28]. A logarithmic fitting was also made between the exit diameter and the laser power, which matches well with the experimental data. The difference between the inner diameter of the entrance and the exit diameter was further logarithmically correlated with the laser power. Both logarithmic relationships confirm the dominating role that ablation behaviors play in the parameter-compensation strategy presented above. The logarithmic dependence of the exit diameters on laser power also leads to the superior effectiveness of laser-power compensation over scanning-diameter compensation in controlling sidewall tapers.

Further, holes with diameters of 1050 and 950 μm (i.e. 50 μm larger and smaller than those holes above) were machined to show the stability of the parameter-compensation strategy. As highlighted in the green circles in figure 7, the outer and inner diameters of the entrance and exit diameters increase or decrease synchronously by $\sim$50 μm and remain almost equal to each other. It indicates that the parameter compensation can precisely control the hole diameters and be generally used to machine macroscale holes of various sizes. Past investigations on fs laser ablation behaviors were primarily conducted through measuring basic features (e.g. craters and lines) ablated on solid surfaces under various laser conditions for ablation-depth and ablation-threshold analysis [27, 28]. This study succeeded in controlling the fs laser ablation behaviors within actual manufacturing—in particular, the sidewall quality control—and explores the flexibility in controlling both the fs laser energy input and laser-matter interactions to realize high-precision machining.

3.5. Examination of surface quality

The surface finish inside the round holes after completing both Steps 1 and 2 was also examined through SEM at different depth positions. As shown in figure 8(b), the top part of the sidewall is clean and smooth except for the remaining roughness at the entrance within a depth of 50 μm and a lateral width of 10 μm. The top part of the sidewall is covered by discontinuous submicron ripples together with some submicron particles (figure 8(e)), which are both typical structures induced by fs laser processing of metal surfaces [29, 30]. The middle part of the sidewall is more uniform (figure 8(c)), mainly covered by submicron particulates (figure 8(f)). Since the laser focal spot was only forwarded to a depth of 500 μm in Step 1 to save the entire machining time, the bottom part of the sidewall was not uniformly ablated by the fs laser focal spot, resulting in light tracks of fs laser propagation along the Z-direction (figure 8(d)). In spite of this, figure 8(g) indicates that the tracks are also covered by the fs laser induced submicron features, showing no microscale surface roughness.

The formation of nanoscale features, particularly ripples, on sidewalls of fs laser machined holes and cavities has been previously reported [10, 11, 31, 32]. The orientation of ripples is mainly determined by the polarization conditions of fs lasers and also affected by other machining conditions. In this research, it is believed that the laser rotating along spiral circles in Step 1 primarily accounts for the formation of ripples, while the continuous and high-speed refining in Step 2 accounts for both the formation of submicron particulates and the discontinuity of the ripples. Since the laser focal spot was only forwarded to a depth of 500 μm in Step 1, ripples were more obvious on the top part of the sidewall and remained there after Step 2. From top to bottom of the sidewall, the influence of Step 2 becomes more obvious, producing more prominent particulate features. Regardless of the surface features, the quality examinations verify that the parameter-compensation strategy using the 5-axis scanner can

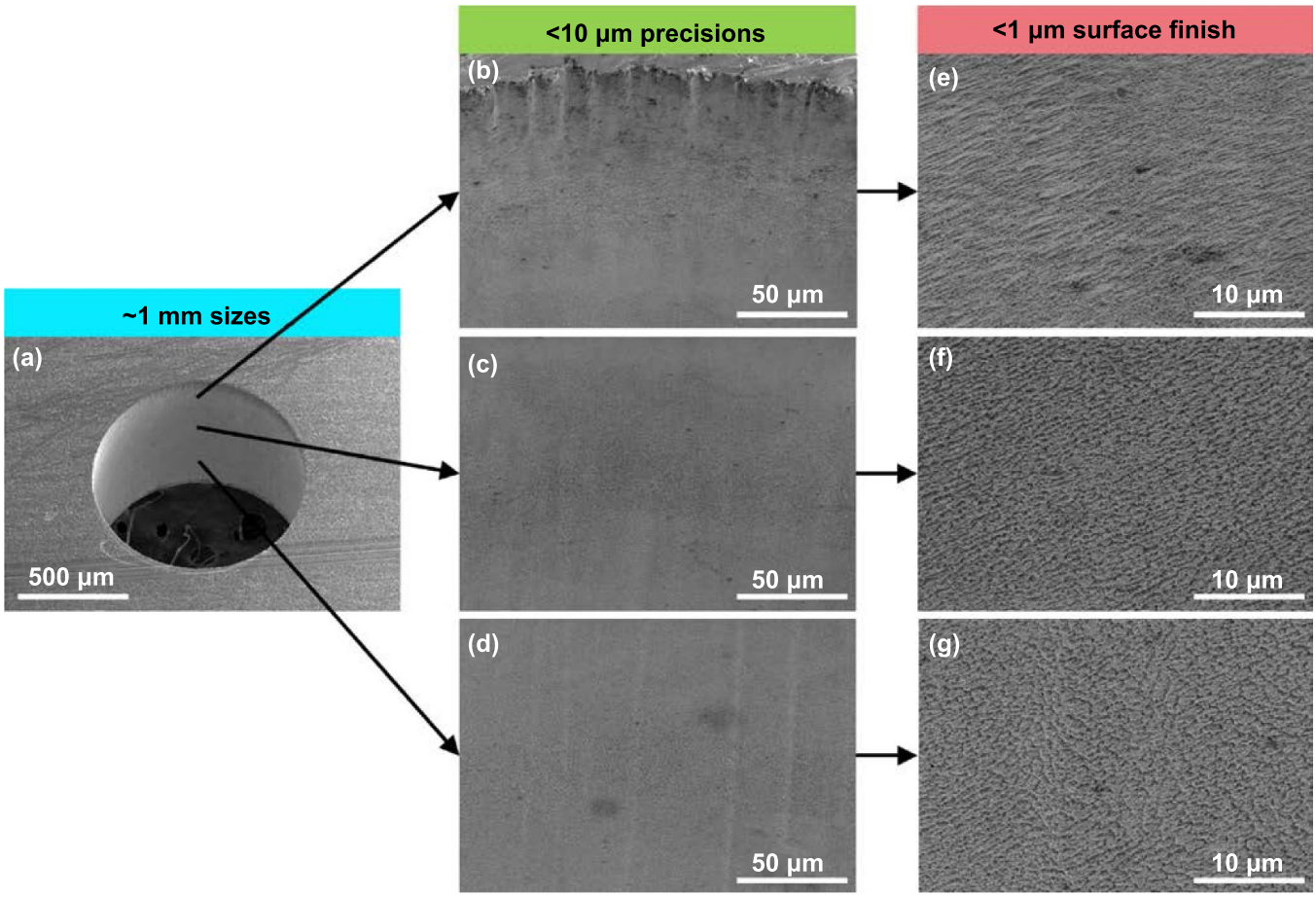

Figure 8. SEM images at different sidewall positions showing the quality of the hole sidewall machined with the optimized scanning-diameter and laser-power compensations. (a) Overview SEM of a hole with a 1 mm diameter and 1 mm depth. (b)–(d) Zoomed SEMs of the top, middle, and bottom parts of the sidewall, respectively. (e)–(g) Magnified images of (b)–(d), showing the fs laser-induced submicron surface features.

machine mm-scale holes with the capability of controlling their geometries with precisions <10 μm and surface finishes with roughness <1 μm.

3.6. Evolutions of entrances and exits

To demonstrate the effect of the AOI control and the parameter compensation more clearly, the representative results machined under different conditions are summarized in figure 9 for comparison:

(a) As discussed earlier, vertical sidewalls can be produced at an AOI of 0° with the 5-axis scanner but accompanied by noticeably rough edges of large chamfers indicated by ring-shaped features at the entrances (figure 9(a)).
(b) Through merely applying larger AOIs to minimize the impact of beam divergence, the edges at the entrances can be effectively reduced (figure 9(c)) but at a cost of increased sidewall tapers, which are indicated by two concentric circles observed from the exits. The larger and smaller circles represent the exit and the inner diameters of the entrances, respectively (figure 9(d)).
(c) The scanning-diameter compensation was first applied to simultaneously control both sidewalls and edges. The sidewall tapers resulting from larger AOIs are reduced, indicated by a narrower gap between the two circles representing the exit and the inner diameters of the entrances (figure 9(f)). However, the effect of scanning-diameter compensation saturates after reducing the gaps between the exit and the inner diameters of the entrances by around 40 μm and, thus, is not sufficient to completely eliminate the sidewall tapers.
(d) Through applying both the scanning-diameter and laser-power compensations, the sidewall tapers are further reduced (figure 9(h)). When the scanning-diameter compensation is fixed, the sidewall taper obviously decreases when more laser-power compensation is used and eventually becomes unnoticeable (figure 9(j)). Meanwhile, the entrances remain sharp and smooth (figures 9(g) and (i)), and the edge widths at the entrances remain below 10 μm.
(e) As a comparison, excessive laser-power compensation causes smaller diameters at the exits than at the entrances, indicated by two smooth and concentric circles observed from the entrances. The larger and smaller

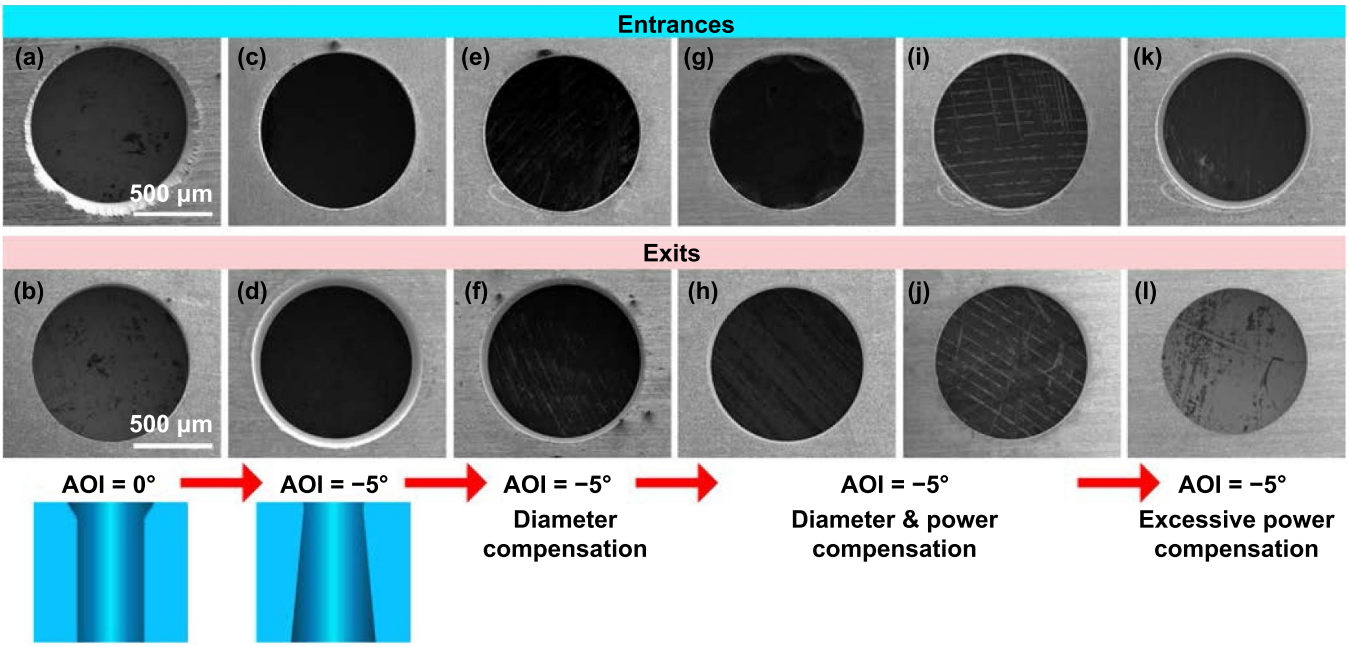

Figure 9. A comparative summary of holes machined under different conditions, showing the evolution of hole entrances (top-row SEMs) and exits (bottom-row SEMs). (a), (b) AOI = 0°, without parameter compensation; (c), (d) AOI = −5°, without parameter compensation; (e), (f) AOI = −5°, with only scanning-diameter compensation; (g), (h) AOI = −5°, with both scanning-diameter and laser-power compensations; (i), (j) AOI = −5°, with scanning-diameter and more laser-power compensations; (k), (l) AOI = −5°, with scanning-diameter and excessive laser-power compensations.

circles represent the entrances and the exits, respectively (figure 9(k)).

Such evolution presents how the geometrical profiles and edge qualities are finely manipulated through AOI control and parameter compensation, providing an effective solution for machining macroscale holes requiring micro/nanoscale precisions. In addition to AOI which is most commonly used to tune tapers, this research indicates that controlling the fs laser ablation behaviors via parameter compensation can also realize tuning of sidewall tapers from positive to negative. Besides, it is worth noting that all experiments in this research were tested to show high repeatability.

3.7. Machining diverse and complex geometries

In addition to round holes, the AOI control and parameter compensation can also be used to machine complex geometries of macroscale sizes. For example, an elliptical hole (1 mm deep, 1 mm/500 μm wide in its major/minor axes) was machined using an AOI of −5°, a diameter compensation of 400 μm, and a laser power of 5.6 W, the same as the optimized parameters for machining the round holes. No ring-like features on the entrance or concentric circles on the exit were observed (figure 10(a)), indicating that both a vertical sidewall and sharp edges were realized simultaneously. Furthermore, the same processing conditions were used to machine free-shaped geometries, e.g. a combination of two-crossed ellipses (figure 10(b)) and a dumbbell-like geometry with two round holes and a bridge connecting them (figure 10(c)). In spite of their complex shapes, vertical sidewalls along with sharp, clean entrances and exits were achieved on all parts of these geometries. The 3D profiling images collected by the laser scanning microscope further confirm their high-precision geometries with high-quality edges and sidewalls. The success in machining such free-shaped geometries verifies that AOI control and the parameter-compensation strategy developed in this research has no obvious dependence on the geometries to be machined and, thus, can be used as a general approach to macroscale machining.

4. Conclusions

In this research, the key challenge in fs laser macroscale machining (i.e. achieving vertical sidewalls and sharp edges simultaneously) was addressed through developing an fs laser sharp shaping approach with controlled AOI and parameter compensation using a 5-axis scanner. The 5-axis scanner produced vertical sidewalls at an AOI of 0° with obviously rough edges of large chamfers. By applying larger AOIs, the edges at the entrances were reduced, however, at a cost of increased sidewall tapers. Using AOI control and parameter compensation, we succeeded in achieving vertical sidewalls as well as sharp entrances and exits simultaneously for geometries of different shapes with both mm-scale dimensions and depths. The dimensional precisions were controlled below 10 μm while the surface finish was controlled below 1 μm

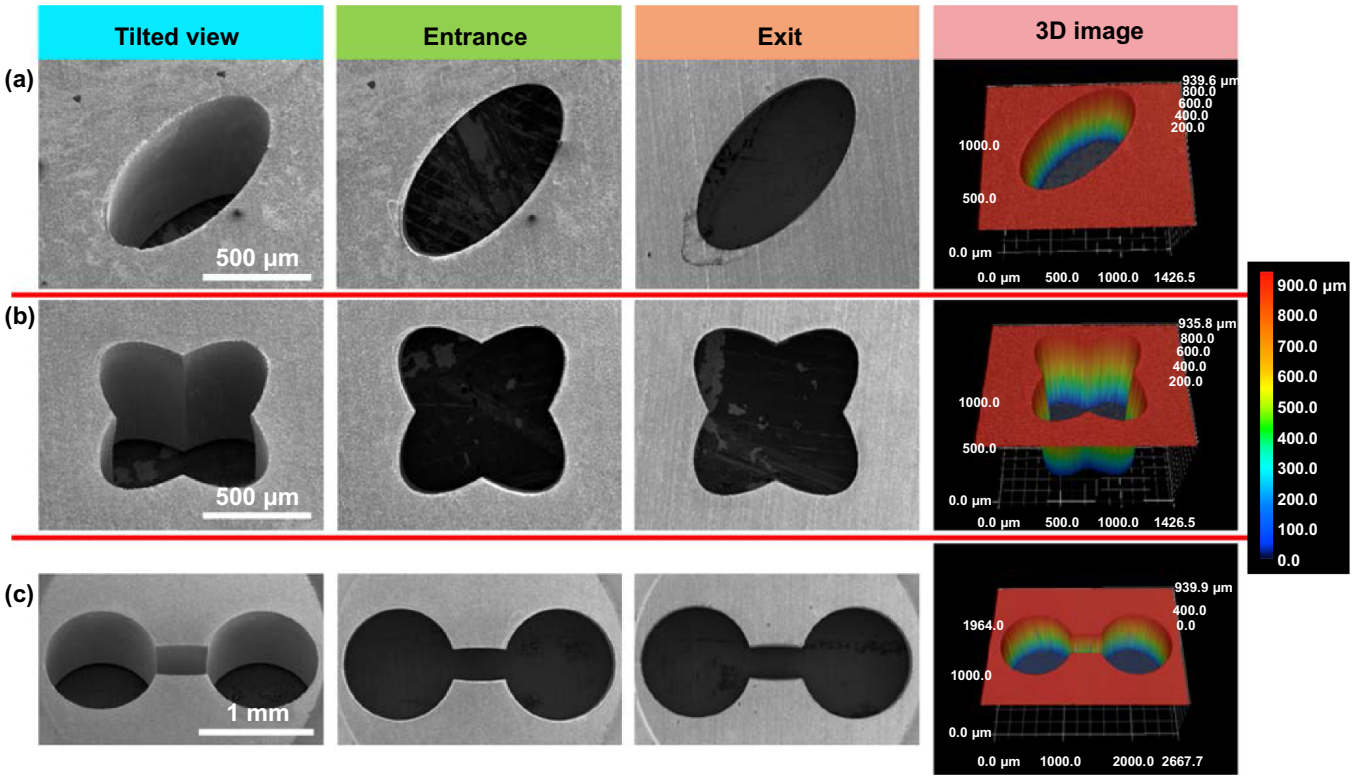

Figure 10. Geometries of different shapes with non-tapered sidewalls and sharp edges. (a)–(c) SEM and 3D profiling images of a single ellipse, two crossed ellipses, and a dumbbell-like geometry, respectively.

in roughness. The laser-power compensation plays a dominating role in achieving non-tapered sidewalls when using larger AOIs. This research presents a novel strategy to finely control the fs laser machining process and establishes the capability of fs lasers in macroscale machining with micro/nanoscale precisions.

Acknowledgments

This study was supported by the National Science Foundation (CMMI 1826392) and the Nebraska Center for Energy Sciences Research (NCESR). The research was performed in part in the Nebraska Nanoscale Facility: National Nanotechnology Coordinated Infrastructure and the Nebraska Center for Materials and Nanoscience, which are supported by the National Science Foundation under Award ECCS: 1542182, and the Nebraska Research Initiative. The authors thank Jamie Eske for her help editing the manuscript.

Conflict of interest

The authors declare no conflicts of interest.

ORCID iDs

Peixun Fan https://orcid.org/0000-0002-8600-7179
Jean-François Silvain https://orcid.org/0000-0002-5881-6833

References

[1] Qin L *et al* 2020 5 nm nanogap electrodes and arrays by super-resolution laser lithography *Nano Lett.* **20** 4916–23
[2] Saha S K, Wang D E, Nguyen V H, Chang Y N, Oakdale J S and Chen S C 2019 Scalable submicrometer additive manufacturing *Science* **366** 105–9
[3] Chen Y and Xiong S S 2020 Directed self-assembly of block copolymers for sub-10 nm fabrication *Int. J. Extreme Manuf.* **2** 032006
[4] Kerse C *et al* 2016 Ablation-cooled material removal with ultrafast bursts of pulses *Nature* **537** 84–88
[5] Ródenas A, Gu M, Corrielli G, Paiè P, John S, Kar A K and Osellame R 2019 Three-dimensional femtosecond laser nanolithography of crystals *Nat. Photon.* **13** 105–9
[6] Žemaitis A, Gečys P, Barkauskas M, Račiukaitis G and Gedvilas M 2019 Highly-efficient laser ablation of copper by bursts of ultrashort tuneable (fs-ps) pulses *Sci. Rep.* **9** 12280
[7] Sugioka K and Cheng Y 2014 Ultrafast lasers—reliable tools for advanced materials processing *Light Sci. Appl.* **3** e149
[8] Gan Z S, Cao Y Y, Evans R A and Gu M 2013 Three-dimensional deep sub-diffraction optical beam lithography with 9 nm feature size *Nat. Commun.* **4** 2061
[9] Li Z Z, Wang L, Fan H, Yu Y H, Chen Q D, Juodkazis S and Sun H B 2020 O-FIB: far-field-induced near-field breakdown for direct nanowriting in an atmospheric environment *Light Sci. Appl.* **9** 41
[10] Romoli L and Vallini R 2016 Experimental study on the development of a micro-drilling cycle using ultrashort laser pulses *Opt. Lasers Eng.* **78** 121–31
[11] Romoli L, Rashed C A A and Fiaschi M 2014 Experimental characterization of the inner surface in micro-drilling of spray holes: a comparison between ultrashort pulsed laser and EDM *Opt. Laser Technol.* **56** 35–42

[12] Li Q, Yang L J, Hou C J, Adeyemi O, Chen C Y and Wang Y 2019 Surface ablation properties and morphology evolution of K24 nickel based superalloy with femtosecond laser percussion drilling *Opt. Lasers Eng.* **114** 22–30
[13] Zhang Z F, Wang W H, Jiang R S, Zhang X B, Xiong Y F and Mao Z 2020 Investigation on geometric precision and surface quality of microholes machined by ultrafast laser *Opt. Laser Technol.* **121** 105834
[14] Zhao J, Wang W J, Wang R J and Cui J L 2018 Machining millimeter-scale deep holes in SiC_f/SiC material using femtosecond laser filamentation effect *Mater. Sci. Adv. Compos. Mater.* **2** 1
[15] Žemaitis A, Gaidys M, Gečys P, Barkauskas M and Gedvilas M 2021 Femtosecond laser ablation by bibursts in the MHz and GHz pulse repetition rates *Opt. Express* **29** 7641–53
[16] Li T, Ren N F, Wang H X, Zhou W, Wu N E, Xia K B, Xu Y and Tian J N 2020 Femtosecond laser layered ring trepanning of stainless steel sheets with and without transverse magnetic assistance *Opt. Laser Technol.* **129** 106231
[17] Wang R J, Dong X, Wang K D, Sun X M, Fan Z J and Duan W Q 2019 Two-step approach to improving the quality of laser micro-hole drilling on thermal barrier coated nickel base alloys *Opt. Lasers Eng.* **121** 406–15
[18] Liu Y S, Zhang R H, Li W N, Wang J, Yang X J, Cheng L F and Zhang L T 2018 Effect of machining parameter on femtosecond laser drilling processing on SiC/SiC composites *Int. J. Adv. Manuf. Technol.* **96** 1795–811
[19] Wang Q X, Chen A M, Li S Y, Qi H X, Qi Y, Hu Z and Jin M X 2015 Influence of ambient pressure on the ablation hole in femtosecond laser drilling Cu *Appl. Opt.* **54** 8235–40
[20] Wang M L, Yang L J, Zhang S and Wang Y 2018 Experimental investigation on the spiral trepanning of K24 superalloy with femtosecond laser *Opt. Laser Technol.* **101** 284–90
[21] Li F P, Feng G, Yang X J, Li X G, Ma G and Lu C J 2020 Research on microhole processing technology based on the femtosecond-laser spiral trepanning method *Appl. Sci.* **10** 7508
[22] Tan Y X, Chu W, Wang P, Li W B, Wang Z and Cheng Y 2019 Water-assisted laser drilling of high-aspect-ratio 3D microchannels in glass with spatiotemporally focused femtosecond laser pulses *Opt. Mater. Express* **9** 1971–8
[23] Auerswald J, Ruckli A, Gschwilm T, Weber P, Diego-Vallejo D and Schluter H 2016 Taper angle correction in cutting of complex micro-mechanical contours with ultra-short pulse laser *J. Mech. Eng. Autom.* **6** 334–8
[24] Mincuzzi G, Faucon M and Kling R 2019 Novel approaches in zero taper, fast drilling of thick metallic parts by ultra-short pulse laser *Opt. Lasers Eng.* **118** 52–57
[25] Wang M L, Mei W and Wang Y 2019 Simulation of femtosecond laser ablation sapphire based on free electron density *Opt. Laser Technol.* **113** 123–8
[26] Davydov R V and Antonov V I 2018 Computer simulation of femtosecond pulsed laser ablation of aluminium and copper *J. Phys.: Conf. Ser.* **1124** 081037
[27] Garcia-Lechuga M, Gebrayel El Reaidy G, Ning H, Delaporte P and Grojo D 2020 Assessing the limits of determinism and precision in ultrafast laser ablation *Appl. Phys. Lett.* **117** 171604
[28] Miyasaka Y, Hashida M, Nishii T, Inoue S and Sakabe S 2015 Derivation of effective penetration depth of femtosecond laser pulses in metal from ablation rate dependence on laser fluence, incidence angle, and polarization *Appl. Phys. Lett.* **106** 013101
[29] Fan P X, Pan R and Zhong M L 2019 Ultrafast laser enabling hierarchical structures for versatile superhydrophobicity with enhanced Cassie–Baxter stability and durability *Langmuir* **35** 16693–711
[30] Zhang Y Y, Jiao Y L, Li C Z, Chen C, Li J W, Hu Y L, Wu D and Chu J R 2020 Bioinspired micro/nanostructured surfaces prepared by femtosecond laser direct writing for multi-functional applications *Int. J. Extreme Manuf.* **2** 032002
[31] Racine V, Le Barh M, Killaire G and Weck A 2019 Effect of polarization on ripple formation in deep femtosecond laser machined cavities *J. Mater. Process. Technol.* **271** 162–71
[32] Hu Y W *et al* 2016 LIPSS formed on the sidewalls of microholes in stainless steel trepanned by a circularly polarized femtosecond laser *Appl. Phys.* A **122** 665